Structure, bonding, and possible superhardness of CrB_4

Haiyang Niu,[1] Jiaqi Wang,[1] Xing-Qiu Chen,[1,*] Dianzhong Li,[1] Yiyi Li,[1] Petr Lazar,[2,3]
Raimund Podloucky,[2] and Aleksey N. Kolmogorov[4]

[1]*Shenyang National Laboratory for Materials Science, Institute of Metal Research, Chinese Academy of Sciences, Shenyang 110016, China*
[2]*Center for Computational Materials Science, University of Vienna, Sensengasse 8, A-1090 Vienna, Austria*
[3]*Regional Centre of Advanced Technologies and Materials, Department of Physical Chemistry, Faculty of Science, Palacky University Olomouc, Tr. 17. Listopadu 12, 771 46 Olomouc, Czech Republic*
[4]*Department of Materials, University of Oxford, Parks Road, Oxford OX1 3PH, United Kingdom*

(Received 9 August 2011; revised manuscript received 13 April 2012; published 25 April 2012)

By electron and x-ray diffraction we establish that the CrB_4 compound discovered over 40 years ago crystallizes in the $oP10$ (*Pnnm*) structure, in disagreement with previous experiments but in agreement with a recent first-principles prediction. The 3D boron network in this structure is a distorted version of the rigid carbon sp^3 network proposed recently for the high-pressure C_4 allotrope. Our systematic density functional theory analysis of the electronic, structural, and elastic properties in ten related transition metal TMB_4 tetraborides (TM = Ti, V, Cr, Mn, Fe and Y, Zr, Nb, Mo, Tc) identifies CrB_4 as the prime candidate to be a superhard material. In particular, the compound's calculated weakest shear and tensile stresses exceed 50 GPa, and its Vickers hardness is estimated to be 48 GPa. We compare the reported and estimated Vickers hardness for notable (super)hard materials and find that the CrB_4 calculated value is exceptionally high for a material synthesizable under standard ambient-pressure conditions.

DOI: 10.1103/PhysRevB.85.144116 PACS number(s): 62.40.+i, 62.20.Qp, 63.20.dk, 71.20.Be

I. INTRODUCTION

Covalent networks with high atomic densities and three-dimensional (3D) morphologies[1–5] are basic features of most of the known superhard materials, including diamond [Fig. 1(a)], c-BC_2N, c-BN, and the recently found compounds c-BC_5[6] and γ-B_{28}.[7–9] A series of promising superhard allotropes of carbon with strong quasi-sp^3 covalent bonding as realized in a monoclinic (S-carbon[10] and M-carbon[11]), tetragonal body-centered (bct-C_4[12,13]), and orthorhombic (R-carbon,[10] P-carbon,[10] and W-carbon[14]) structure have been proposed for the interpretation of the x-ray diffraction pattern of cold-compressed graphite.[15] In particular, metastable bct-C_4 is built up by an unusual framework[10] of interconnected square C_4 units [Fig. 1(b)] and has been predicted to be superhard by several first-principles studies.[16–19] Inspired by the search for superhard materials which can be fabricated without the need of an expensive high pressure[20] or a chemical vapor deposition[21] methods, we re-examine a known stable intermetallic CrB_4 compound comprised of similar B_4 units. We find that, compared to the ReB_2 compound shown recently to have a remarkably high hardness,[20,22–24] CrB_4 holds the promise to have even more outstanding mechanical properties.

First we characterize CrB_4 experimentally by means of electron diffraction (ED) and x-ray diffraction (XRD) techniques confirming a first-principles prediction[25,26] that the orthorhombic structure of CrB_4, originally suggested to have the $Immm$ space group [with the $oI10$ unit cell in Pearson notation, see Fig. 1(c)], has a lower-symmetry $Pnnm$ space group [$oP10$, see Fig. 1(d)]. On the basis of density functional theory (DFT) calculations,[27–30] we establish that CrB_4 with the newly claimed structure has lowest ideal tensile and shear strengths of 51 GPa, which are comparable to those of cubic boron nitride (c-BN). Making use of an empirical model[31,32] correlating the elastic moduli and Vickers hardness (H_v), we estimate $H_v \approx 48$ GPa, which exceeds significantly the 40 GPa threshold of superhardness. To rationalize this finding we perform a DFT study of the ten transition metal borides, TMB_4 (with TM = Ti, V, Cr, Mn, Fe as well as TM = Zr, Nb, Mo, Tc, Ru). Our results indicate that the atomic size and valence of the TM elements play a key role in determining the mechanical properties. The hardness reaches a maximum for TM = Cr when all bonding B quasi-sp^3 and hybridized Cr-B states become occupied.

In 1968, Andersson and Lundström[33] reported the synthesis of CrB_4 and characterized it as an orthorhombic $oI10$ structure. Given the very good fit of the x-ray pattern to the $oI10$ structure and the recently demonstrated elastic stability of the compound[34] there was no reason to suspect incompleteness of this structural model. However, examination of the ground states of Fe-B[25] and Cr-B systems[26] revealed a dynamical instability of the $oI10$ structure due to phonon modes with an imaginary frequency near $\mathbf{q} = \mathbf{0}$. As a consequence, the boron framework undergoes a significant distortion transforming the orthorhombic body-centered structure ($oI10$) into a primitive one ($oP10$). It was noted[26] that this structural transformation leaves the unit cell dimensions and the XRD patterns essentially unchanged, which necessitates the use of an alternative characterization technique to finally resolve the structure of CrB_4.

II. EXPERIMENTAL AND COMPUTATIONAL DETAILS

A 20 g sample with the initial composition of CrB_4 was prepared by repeated arc-melting of electrolytic chromium (from Alfa Aesar, claimed purity 99.997%) and crystalline boron pieces (from Alfa Aesar, claimed purity 99.5%) under argon atmosphere. Cut sample pieces were sealed in quartz under argon and annealed in a high temperature furnace for 192 hours at 1250 °C. The annealed samples were characterized via metallographic microscope (LEISS Axiovert 200 MAT),

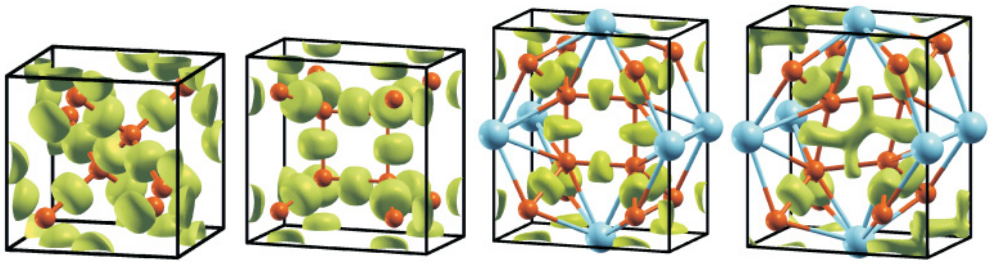

(a) $Fd\bar{3}m$ ($cF8$) (b) I_4/mmm ($tI8$) (c) $Immm$ ($oI10$) (d) $Pnnm$ ($oP10$)

FIG. 1. (Color online) Isosurfaces of the electron localization function (ELF),[35] corresponding to a value of 0.75. (a),(b) Diamond and bct-C_4 carbon; (c),(d) orthorhombic structures of CrB_4. Small and large balls denote B and Cr atoms, respectively.

scanning electron microscope (SEM, HITACHI S-3400N) in the back-scattered electron mode (BSE). Our electron probe microanalyser (EPMA, SHIMADZU EPMA-1610) results showed 20.374 at.% and 79.626 at.% elemental compositions of Cr and B, respectively. The presence, distribution, and phase characteristics of CrB_4 (78.06%), CrB_2 (7.32%), and amorphous boron (14.62%) were further analyzed with an electron backscatter diffraction (EBSD) micrograph. The annealed samples were characterized via metallographic microscope (LEISS Axiovert 200 MAT), scanning electron microscope (SEM, HITACHI S-3400N) in the back-scattered Electron mode (BSE). The grain sizes of CrB_4 and CrB_2 are about 100 μm according to our electron backscatter diffraction (EBSD) micrograph. However, the available analyzing area of TEM is only about 1 μm, which also show nice grain boundary between boron and CrB_4. Although it is very difficult to use TEM image to analyze overall grain sizes and areas of amorphous boron and crystalline CrB_4, it is enough to analyze the presence, distribution, and phase characteristic of the annealed sample by EBSD micrograph. Our electron probe microanalyser (EPMA, SHIMADZU EPMA-1610) results show the presence, distribution, and phase characteristics of CrB_4 (78.06%), CrB_2 (7.32%), and amorphous boron (14.62%) in the annealed samples. Among them, the amorphous boron cannot be detected by XRD. TEM characterization of finely ground samples was carried out with Tecnai G2 F20 S-TWIN transmission electron microscope. For TEM measurement, the annealed samples (3 mm rods) were first cut into small pieces with a thickness of 500 μm, ground first with various grit silicon carbide papers, polished with diamond paste of 3.5 μm to a thickness around 50 μm, further ground by dimple grinder to a thickness of about 20 μm, and finally thinned precisely by ion polishing system. Finally, we obtained XRD patterns using a Rigaku diffractometer and Cu K_a irradiation ($\lambda = 1.54056$ Å) and performed full Rietveld refinement using the FULLPROF package.[36]

For DFT calculations we used the Perdew-Burke-Ernzerhof exchange-correlation functional[27] within the generalized gradient approximation and the projector-augmented waves method[28] as implemented in VASP.[29,30] The energy cutoff was set at 500 eV. We allowed spin polarization for all TMB_4, but only one compound of MnB_4 showed a small nonzero magnetic moment of about 0.7 μ_B per Mn in the antiferromagnetic ordering. A very accurate optimization of structural parameters was achieved by minimizing forces (below 0.001 eV/Å) and stress tensors (typically below 0.5 kB). Well-converged results were obtained utilizing a dense $9 \times 9 \times 11$ $\vec{k}$-point grid for the Brillouin zone integration. The elastic constants of orthorhombic TMB_4 were derived from the total energy as a function of suitable lattice distortions.[37] These strain energies were fitted to third-order polynomials from which the elastic constants at the equilibrium volume were derived. For calculating the tensile and shear strength, we employed the method described in Refs. 38–40. The lattice vectors were incrementally deformed in the direction of the applied stress. At each step of incremental strain, we allowed a full relaxation of the unit cell shape and the strain components orthogonal to the direction of the applied stress.

III. STRUCTURAL REFINEMENTS

Figure 2 shows our experimental ED patterns projected along the [100], [110], [111], and [101] directions revealing that the unit cell has the dimensions $|a^*| \approx 2.1$ nm^{-1}, $|b^*| \approx 1.8$ nm^{-1}, $|c^*| \approx 3.5$ nm^{-1} and it can be classified as a primitive orthorhombic lattice. The simulated ED pattern along [101] for the $oP10$ structure [Fig. 2(f)] shows additional reflections as compared to $oI10$ [Fig. 2(d)], which is expected because the unit cell is doubled and the number of symmetry operations is reduced from 16 to 8. The corresponding extra reflections are clearly present in the observed [101] pattern which unambiguously points at the $oP10$ structure. The $oP10$ structural model was further used to refine the powder XRD data in Table I.

IV. FIRST-PRINCIPLES CALCULATIONS

To elucidate the stabilization role of the *TM* atom we carried out a series of DFT calculations for ten TMB_4 compounds. Figure 3 is a compilation of the energy-versus-volume curves for 3*d*- and 4*d*-series TMB_4. One can see that the five compounds [including three 3*d* compounds (CrB_4, MnB_4, FeB_4) and two 4*d* compounds (TcB_4 and RuB_4)] are more stable in the distorted $oP10$ structure, and the other five compounds prefer to remain in the nondistorted $oI10$ structure. For CrB_4, the theoretical lattice constants and internal atomic parameters are also compiled in Table I, evidencing a nice agreement with the experimental refinements. From Fig. 3, it is also noticeable that the structural transformation is accompanied by a volume reduction. Finally, by artificially decreasing (increasing) the volume one can induce (disfavor)

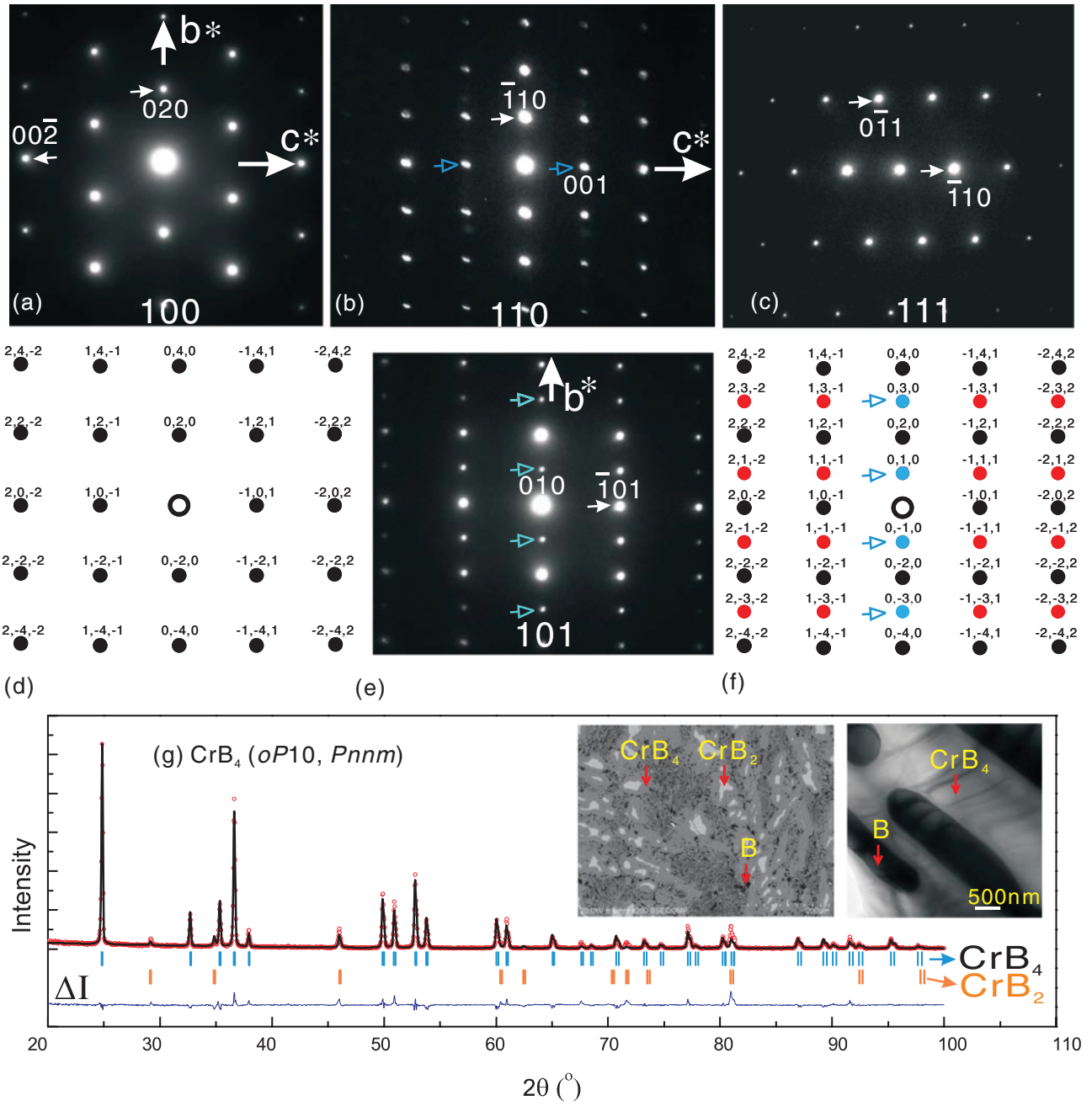

FIG. 2. (Color online) (a)–(c),(e) Experimental electron diffraction (ED) patterns along the [100], [110], [111] and [101] directions, respectively. (d), (f) Theoretical [101] ED patterns for $oI10$ and $oP10$ structures, respectively; (g) Rietveld refinement (Cu $K_{\alpha 1}$) of the experimental x-ray diffraction data; reflections of CrB_2 are indicated by vertical bars. Hollow arrows in (b),(e),(f) denote the second-order diffraction spots. Left inset in (g) shows an EBSD micrograph of sample annealed at 1250 °C and eight days. Note that amorphous boron could not be detected by XRD pattern. Right inset in (g) is a TEM image showing the phase boundary of CrB_4.

the distortion for all the considered TMB_4 compounds. In order to demonstrate the significance of various factors determining the $oI10 \rightarrow oP10$ structural transformation we compared the energies gains, ΔE_{dist} and ΔE_{full}, obtained in two different settings: (1) the lattice constants of $oI10$ were kept fixed and the internal coordinates with the $oP10$ distortion were relaxed, and (2) the $oP10$ unit cells were fully relaxed. The results summarized in Table II show that the energy gained by the $oI10$ to $oP10$ transformation is larger for the $3d$ compounds and increases within both series from left to right. Most of the energy gain (over 90% in the $3d$ series and over 79% in the $4d$ series) comes from the distortion of the boron network.

The mechanism causing the observed distortion in CrB_4 is many fold, because it is related to the quasi-sp^3 B-B bonding, the hybridization of the B- and Cr-like states, the atomic size of Cr relative to the available volume in the B cage, and the charge transfer between B and Cr (i.e., the valencies). It is illustrative to look first at the evolution of the B network in the sequence of the related structure types: diamond, bct-C_4, $oI10$, and $oP10$ (see Fig. 1). In diamond,

TABLE I. Experimental crystal structural parameters (a, b, c in Å) of CrB_4 with the $oP10$ (Pnnm, No. 58) structure at room temperature (Expt) in comparison with the theoretical first-principles calculation at 0 K (DFT). X-ray refinement has been performed with the program FULLPROF[36] based on the $oP10$ structural model as illustrated by DFT and experimental electronic diffraction images. Reliability factors: $R_F = 8.98\%$.

Lattice	a	b	c		
Expt	4.7452(3)	5.4764(3)	2.8662(2)		
DFT	4.7247	5.4756	2.8474		
Atoms	Site	x	y	z	Biso
Cr (Expt)	2c	0	0	0	0.53
Cr (DFT)	2c	0	0	0	
B (Expt)	4g	0.1643	0.6331	0	0.44
B (DFT)	4g	0.1638	0.6326	0	
B (Expt)	4g	0.2236	0.3209	0	0.77
B (DFT)	4g	0.2238	0.3208	0	

the tetrahedral arrangement of four nearest neighbors with the $\cos^{-1}(-1/3) \approx 109.5^\circ$ angles between the bonds is optimal for the sp^3 hybridization[41] [Fig. 1(a)]. In bct-C_4, the symmetry of the local atomic environment is broken as two bonds form a

TABLE II. Decomposed energy gains (ΔE_{full} and ΔE_{dist} in eV/atom) and the ratio of $\Delta E_{dist}/\Delta E_{full}$ for the $oI10$ to $oP10$ phase transformation for five compounds: three 3d compounds (CrB_4, MnB_4, FeB_4) and two 4d compounds (TcB_4 and RuB_4).

	ΔE_{full}	ΔE_{dist}	$\Delta E_{dist}/\Delta E_{full}$
CrB_4	− 0.00546	− 0.00498	0.911
MnB_4	− 0.01192	− 0.01103	0.925
FeB_4	− 0.02592	− 0.02363	0.912
TcB_4	− 0.00692	− 0.00602	0.870
RuB_4	− 0.01639	− 0.01304	0.796

90° angle [Fig. 1(b)]. In $oI10$, symmetry is further reduced due to the two bonds now having different lengths [namely, 1.73 Å and 1.86 Å for structurally relaxed CrB_4, see Fig. 1(c)]. Finally, in $oP10$ a further deviation from the ideal sp^3 geometry occurs as one of the two nonequivalent B sites has two B-B bonds at an angle well below 90° and the other is no longer four-fold coordinated (a fifth B atom is 2.13 Å away and the electron localization function shown in Fig. 1(d) develops a blob along the short diagonal of the B parallelogram).

Within a semiempirical extended Hückel approach, Burdett *et al.*[42] studied the relative stability of carbon- and boron-based structures by analyzing the moments (μ_n) of the electronic

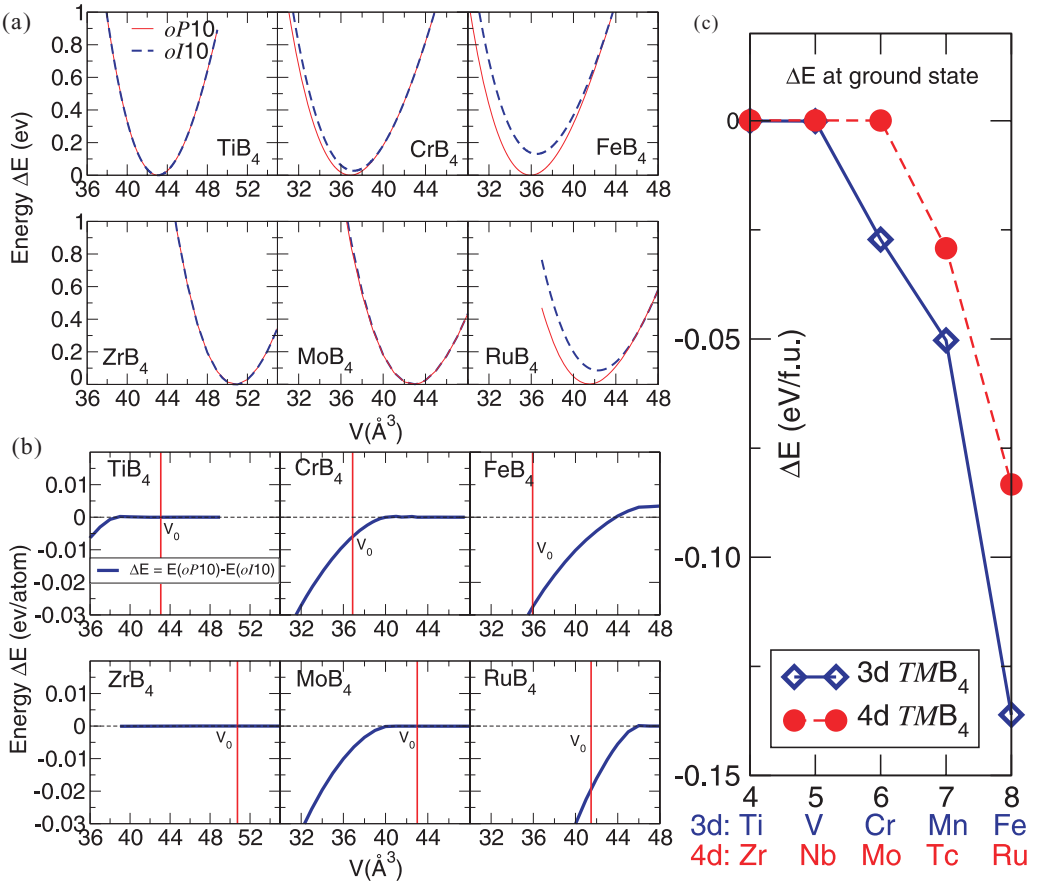

FIG. 3. (Color online) Calculated relative stability of the $oI10$ and $oP10$ structures for ten 3d- and 4d-TMB_4. Panel (a): Energy-versus-volume curves. Panel (b): Relative energy $\Delta E = E(oP10)\text{-}E(oI10)$ as a function of volume (both structures were relaxed at fixed volumes in these tests). The red vertical lines correspond to the equilibrium volume of the fully relaxed $oI10$ or $oP10$ (whichever is more stable for the particular TM). Panel (c): Relative stability as a function of the TM electron count.

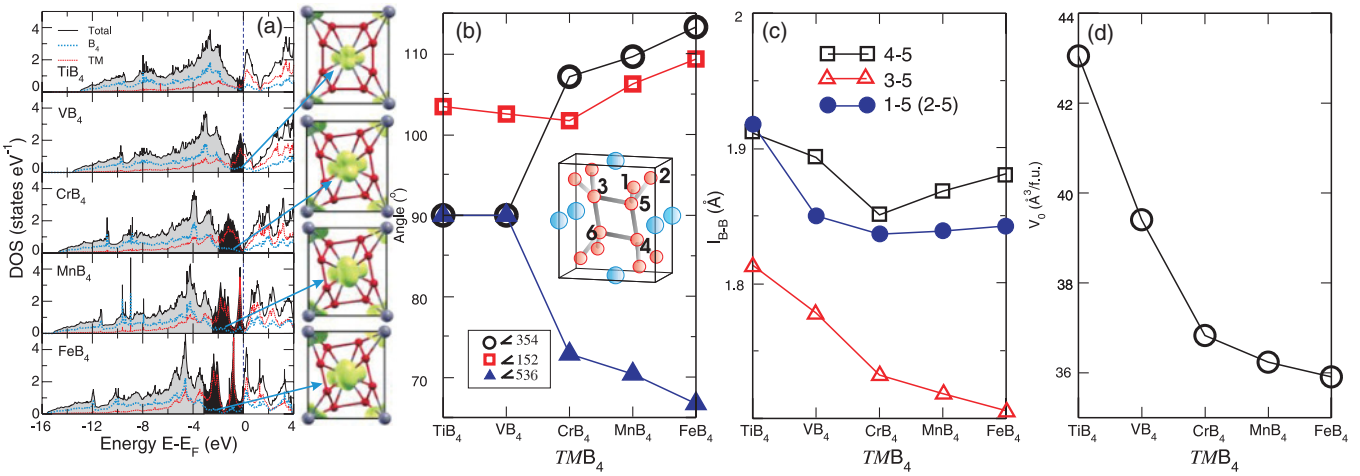

FIG. 4. (Color online) Calculated electronic structure of 3*d*-series TMB_4 compounds (*TM*: 3*d* transition elements). (a) Electronic densities of states with occupied bonding and nonbonding states highlighted in gray and black, respectively. The corresponding insets of structures show charge density isosurfaces (0.1 e/Å ^{3}) for the energy windows corresponding to the nonbonding states. (b)–(e) Variation of bond angles, bond lengths, and atomic volume.[43]

density of states (DOS). They argued that bct-C_4 carbon is less stable than diamond carbon because (i) the nonoptimal 90° angle gives rise to a strain energy and (ii) the four-membered rings result in a higher μ_4 which translates into a more unimodal DOS and a lower stability for elements with a half-filled shell. Their conclusion that the second contribution could stabilize boron-based materials with a lower number of electrons is supported by our DFT calculations: For the group-IV carbon the diamond structure is favored by 0.20 eV/atom while for the group-III boron the bct-C_4 structure is favored by 0.08 eV/atom. The structural differences within the bct-C_4, *oI*10, and *oP*10 family are less pronounced. However, the presence of three-membered rings in *oP*10 may significantly influence the structure's important third and forth DOS moments.

The DOS and formation enthalpies are presented for the more stable of the *oI*10 or *oP*10 structure. For the 3*d* series Fig. 4(a) shows rather similar DOS profiles with the Fermi level (E_F) moving upward as the electron count increases. In the exemplary CrB_4 case, the DOS in the range of (−14, −5) eV is mostly of B-*s*-*p*-like character. The weight of the Cr DOS increases gradually and in the range of (−5, −2) eV a strong hybridization between Cr-d_{xy} (-d_{xz}) and B-p_y (-p_z) states is observed. In the region from −2 to 0 eV the Cr-$d_{(x^2-y^2)}$ and Cr-d_{yz} nonbonding states become dominant. The position of E_F in the pseudogap along with the lowest formation enthalpy achieved for *TM* = Cr [see Fig. 7(c)] is consistent with the prediction[42] of maximum stability occurring in the middle of the 3*d* series. Compared to the calculated DOS in the 3*d* series of TMB_4, the DOS in the 4*d* series shows less distinct separation between the regions with predominantly B-*sp* bonding, strong Cr-*d* and B-*p* hybridization, and pure nonbonding Cr-*d* states [see Fig. 5(a)]. For example, in the

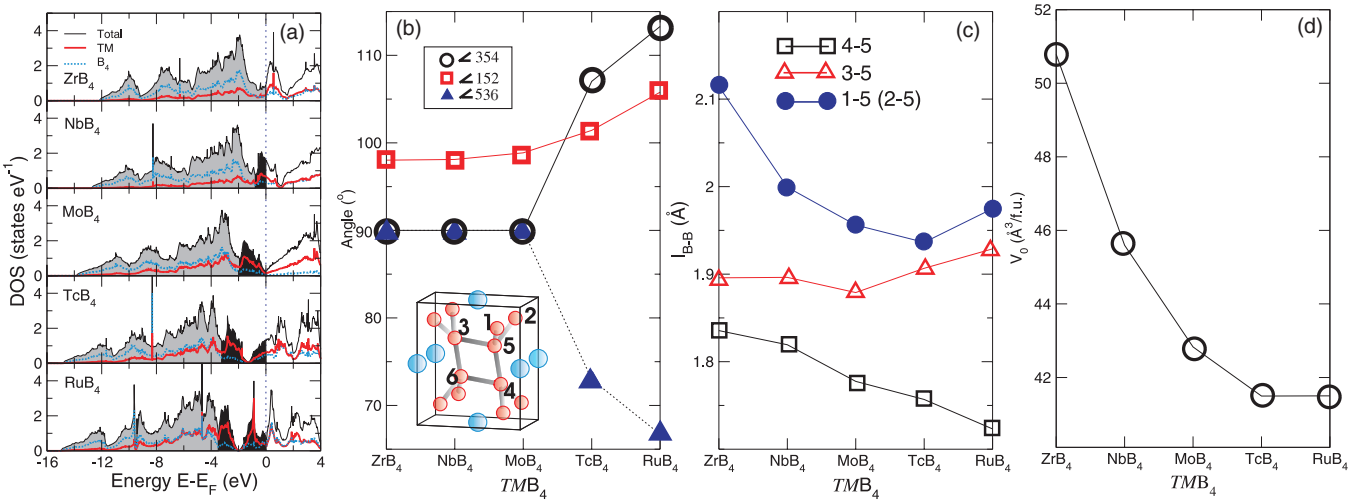

FIG. 5. (Color online) Calculated electronic densities of states for 4*d* TMB_4 at their most stable structures in panel (a). The grey and black regions denote the bonding and nonbonding states, respectively. Panels b, c, and d show the change of distorted angles of boron framework as illustrated by the inset, the change of boron-boron bond length a_{B-B}, the calculated equilibrium volumes (V_0) as a function of *TM*, respectively.

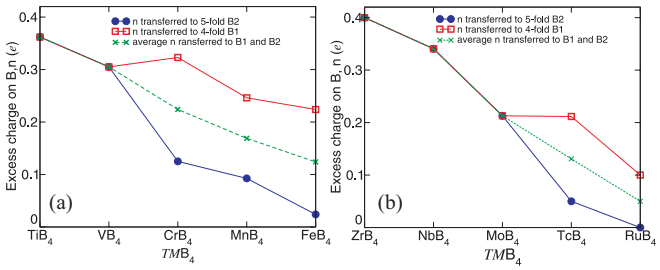

FIG. 6. (Color online) Calculated Bader charges on boron atoms for the 3*d*- and 4*d*-TMB_4 compounds in their respective more stable $oI10$ (TM = Ti, V, Zr, Nb, Mo) or $oP10$ (TM = Cr, Mn, Fe, Tc, Ru) structures. In the $oI10$ structure the boron site is fourfold coordinated whereas in the $oP10$ structure the two nonequivalent boron sites are fourfold (B1) and nearly fivefold (B2) coordinated. The difference in the individual charges on the B1 and B2 atoms might not be very meaningful due to the difficulty of partitioning the charge within the B_4 parallelogram unit. The *average* charge transferred to B1 and B2 shows a systematic, nearly linear trend across the 3*d*- and 4*d* series.

case of $oI10$-MoB_4 the occupied nonbonding states shown as the dark-shaded area are located from 0 to −2 eV, but the projected Mo DOS is comparable to the projected B DOS down to ∼10 eV.

Figures 4(b)–4(d) and 5(b)–5(d) summarize the 3d-series and 4d-series structural trends. Bader decomposition[43] has been performed for ten TMB_4 compounds in their respective more stable $oI10$ or $oP10$ configuration using a very dense $300 \times 300 \times 300$ (27 millions grid points) mesh and the resulting variation of the Bader's charge[43] are shown in Fig. 6. We employ the Bader's charge decomposition to illustrate that the charge transfer from the *TM* element to B (which is around 1 e/*TM*) *decreases* in the sequence from Ti to Fe. Hence, the distortion could be explained by the decreasing number of electrons transferred to B. The derived geometrical result, that three out of four B-B bonds have a minimum bond length for TM = Cr [Fig. 4(c)] demonstrates further why CrB_4 is particularly stable. Considering that E_F in FeB_4 moves from a deep valley in $oI10$ into the shoulder of the antibonding B-*p*-Fe-*d* peak in $oP10$,[25] the optimality of the *p*-*d* bonding appears to be of less importance for the compound's stability (note that the unexpectedly high DOS at E_F in $oP10$-FeB_4 makes the compound a good candidate to be a *phonon-mediated* superconductor with a T_c of 15–20 K[25]).

The mechanical properties of CrB_4 are examined and rationalized via DFT calculation of the elastic properties for the mentioned ten TMB_4 compounds (see Table III). All of them are found to exhibit ultra incompressibility along the *b*-axis and high bulk (B) and sheer (G) moduli. CrB_4 is found to have the highest shear modulus (G = 261 GPa) and Pugh's ratio[44] ($k = G/B = 261/265 = 0.985$), which are two important elastic properties thought to be strongly correlated to hardness.[31] The compound's low Poisson ratio of $v = 0.12$ is typical for materials with strong covalent bonding.[20] Strikingly, the calculated lowest ideal shear and tensile strengths of 51 GPa are remarkably high and comparable to the lowest tensile strength of 55 GPa for superhard *c*-BN.[45] These values exceed considerably the lowest ideal shear strength of 34 GPa[45] in ReB_2 which structure is comprised of buckled 2D boron nets.[46] As a corroboration for a possibly outstanding hardness, by breaking Cr-B bonds along the [001] direction we found the lowest critical cleavage stress[47] of 53 GPa, which matches the lowest ideal strengths. Finally, for estimation of the Vickers hardness (H_v) in terms of elastic properties we employ a recently proposed empirical model,[31,32] $H_v = 2.0(k^2G)^{0.585} - 3.0$ (H_v and G in GPa), which performs well across a large class of materials and hardness values [Fig. 7,

TABLE III. Calculated elastic properties (in GPa) for CrB_4 and known (super)hard materials. The calculated bulk (B) and shear moduli (G) are Reuss-Voigt-Hill averages. The Vickers hardness estimates (H_v^{Calc}) were obtained with our proposed formula (Refs. 31 and 32) using the calculated elastic moduli. Finally, the experimental Vickers hardness values (H_v^{Exp}) for diamond, BC_2N, bct-C_4, c-BN and B_4C were taken from Refs. 31,48, and 50. The elastic constants of CrB_4 are given in both $oI10$ and $oP10$ structures, whereas for the other nine TMB_4 compounds the elastic constants are given only for their corresponding stable ground state phases. In addition, our calculations demonstrated that ZrB_4 is elastically unstable because its C_{44} is negative.

	C_{11}	C_{22}	C_{33}	C_{44}	C_{55}	C_{66}	C_{12}	C_{13}	C_{23}	B	G	H_v^{Calc}	H_v^{Exp}
Diamond	1079			578			124			442	536	95.7	96±5
BC_2N										408	445	75.4	76±2
bct-C_4	933		1190	447		325	172	59		404	421	68.9	
c-BN	820			480			190			400	405	65.2	66±2
B_4C										247	200	31.7	30±2, 31.3–38.9, 42–49
$CrB_4(oP10)$	554	880	473	254	282	250	65	107	95	265	261	48.0	
$CrB_4(oI10)$	591	931	467	252	280	225	64	115	97	275	259	45.1	
$TiB_4(oI10)$	453	739	357	141	242	185	81	114	82	226	190	32.2	
$VB_4(oI10)$	481	812	416	228	277	231	67	115	75	241	237	45.2	
$MnB_4(oP10)$	520	891	507	241	242	224	84	113	91	270	245	41.5	
$FeB_4(oP10)$	381	710	435	218	114	227	137	143	128	253	177	24.2	
$ZrB_4(oI10)$	398	640	277	−63	222	111	107	116	58	199			
$NbB_4(oI10)$	448	757	386	129	256	222	120	148	63	243	194	30.4	
$MoB_4(oI10)$	541	889	494	182	281	249	125	158	72	287	239	36.7	
$TcB_4(oP10)$	481	842	422	180	215	183	143	128	96	266	202	29.4	
$RuB_4(oP10)$	390	785	338	97	179	188	171	195	119	264	148	15.8	

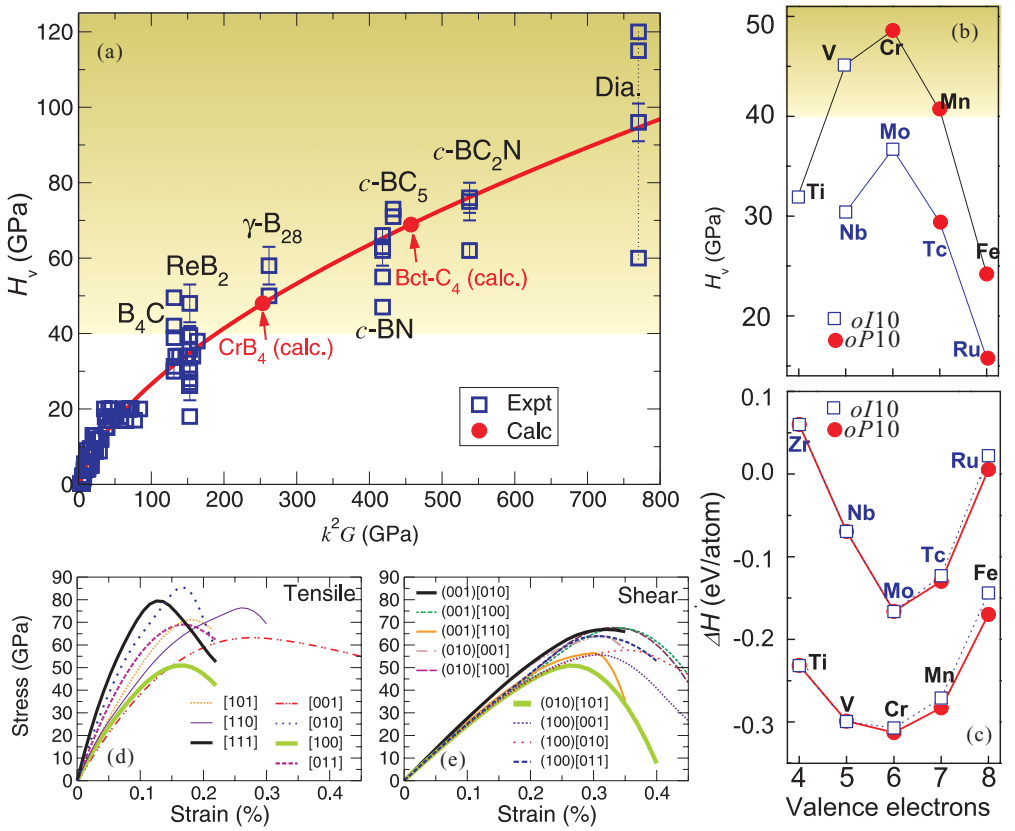

FIG. 7. (Color online) (a) Vickers hardness, H_v, as a function of k^2G, with k being the ratio of the shear (G) to bulk (B) modulus; the experimental data are discussed in Refs. 31 and 32; (b) H_v for the most stable TMB_4 structures derived from the calculated B and G values (see text and Ref. 31); (c) formation enthalpy; (d),(e) ideal tensile and shear strengths of $oP10$-CrB_4.

panel (a)]. Figure 7 reveals that the predicted behavior of H_v for the TMB_4 compounds (panel b) mirrors the trend in their enthalpy of formation (panel c). The largest hardness value of $H_v = 48$ GPa for CrB_4 is well above the superhardness threshold of 40 GPa and decreases rapidly for the considered TMs. In particular, the isoelectronic but larger Mo atom stretches the B network beyond its optimal size, leading to a 25% reduction in hardness. When compared against the known B_4C material which can also be synthesized under ambient pressure, CrB_4 displays (see Table III) superior elastic properties and estimated H_v (note that according to recent measurements B_4C is not superhard in its crystalline form[48]).

V. SUMMARY

Our findings make $oP10$-CrB_4 a prime candidate to be an (up-to-now overlooked) affordable ambient-pressure superhard material. Measurement of the compound's Vickers hardness will be a challenge as pure CrB_4 samples are difficult to produce with standard methods due to the particular behavior of the Cr-B system in the high-temperature–B-rich part of the binary phase diagram.[49] Namely, the cooling of an arc-melted 1:4 elemental mixture leads unavoidably to a two-phase coexistence of CrB_2 and B in a wide high-temperature region from 1830 °C to 1500 °C. Formation of CrB_4 occurs below 1500 °C, but significant fractions of CrB_2 and B can still be present after week(s) of sample annealing, as happened in the original[33] and present studies. Our currently best samples with 78% content of CrB_4 allowed us to reliably characterize the compound's crystal structure but were not suitable for investigation of its mechanical properties. Therefore alternative approaches, such as the powder metallurgical process or the single-crystal growth method, may need to be employed to obtain samples of desired quality.

The confirmation of the new $oP10$ crystal structure of CrB_4 makes the prospect of synthesizing the FeB_4 phase with the same structure—predicted to be a viable high-temperature and high-pressure ground state of the Fe-B system[25,26]—more exciting. Our detailed experimental and theoretical study of the presumably superhard compound CrB_4 demonstrates that materials with appealing properties may still be found in reportedly well-known binary systems.

Note added. While our manuscript was under review, two groups published related studies on CrB_4[51] and on CrB_4/MnB_4.[52] The analysis of the CrB_4 properties in the two studies was carried out only for the unstable $oI10$ structural model which had been shown to be both thermodynamically and dynamically unstable in the Fe-B and Cr-B systems in our previously published work.[25,26]

ACKNOWLEDGMENTS

We thank Xiaobing Hu and Shaobo Mi in the IMR for their valuable help in performing and analyzing ED experiments and Shi Liu for his help in synthesizing experimental samples. We are grateful for support from the "Hundred Talents

Project" of Chinese Academy of Sciences and from NSFC of China (Grand Numbers: 51074151, 51174188) as well as Beijing Supercomputing Center of CAS (including its Shenyang branch in the IMR). A. N. K acknowledges the support from EPSRC CAF EP/G004072/1 in the UK. P.L. acknowledges the support from the Operational Program Research and Development for Innovations - European Social Fund (CZ.1.05/2.1.00/03.0058 and CZ.1.07/2.3.00/20.0017.

*Corresponding author: xingqiu.chen@imr.ac.cn

[1]R. B. Kaner, J. J. Gilman, and S. H. Tolbert, Science **308**, 1268 (2005).
[2]V. V. Brazhkin, A. G. Lyapin, and R. J. Hemley, Philo. Mag. A **82**, 231 (2002).
[3]V. V. Brazhkin, N. Dubrovinskaia, M. Nicol, N. Novikov, R. Riedel, V. Solozhenko, and Y. Zhao, Nat. Mater. **3**, 576 (2004).
[4]J. J. Gilman, Science **261**, 143 (1993).
[5]S. Veprek, J. Nanosci. Nanotechnol. **11**, 14 (2011).
[6]V. L. Solozhenko, O. O. Kurakevych, D. Andrault, Y. L. Godec, and M. Mezouar, Phys. Rev. Lett. **102**, 015506 (2009).
[7]V. L. Solozhenko, O. O. Kurakevych, and A. R. Oganov, J. Superhard Mater. **30**, 428 (2008).
[8]A. R. Oganov, J. H. Chen, C. Gatti, Y. Z. Ma, Y. M. Ma, C. W. Glass, Z. X. Liu, T. Yu, O. O. Kurakevych, and V. L. Solozhenko, Nature (London) **457**, 863 (2009).
[9]E. Y. Zarechnaya, L. Dubrovinsky, N. Dubrovinskaia, Y. Filinchuk, D. Chernyshov, V. Dmitriev, N. Miyajima, A. El Goresy, H. F. Braun, S. Van Smaalen, I. Kantor, A. Kantor, V. Prakapenka, M. Hanfland, A. S. Mikhaylushkin, I. A. Abrikosov, and S. I. Simak, Phys. Rev. Lett. **102**, 185501 (2009).
[10]H. Y. Niu, X.-Q. Chen, S. B. Wang, D. Z. Li, W. L. Mao, and Y. Y. Li, Phys. Rev. Lett. **108**, 135501 (2012).
[11]Q. Li, Y. Ma, A. R. Oganov, H. Wang, H. Wang, Y. Xu, T. Cui, H. K. Mao, and G. Zou, Phys. Rev. Lett. **102**, 175506 (2009).
[12]K. Umemoto, R. M. Wentzcovitch, S. Saito, and T. Miyake, Phys. Rev. Lett. **104**, 125504 (2010).
[13]R. H. Baughman and D. S. Galvao, Phys. Rev. Lett. **104**, 125504 (2010).
[14]J.-T. Wang, C. Chen, and Y. Kawazoe, Phys. Rev. Lett. **106**, 075501 (2011).
[15]W. L. Mao, H.-k. Mao, P. J. Eng, T. P. Trainor, M. Newville, C.-C. Kao, D. L. Heinz, J. F. Shu, Y. Meng, and R. J. Hemley, Science **302**, 425 (2003).
[16]P. Y. Wei, Y. Sun, X.-Q. Chen, D. Z. Li, and Y. Y. Li, Appl. Phys. Lett. **97**, 061910 (2010).
[17]F. M. Gao and X. F. Hao, Phys. Stat. Sol. (RRL) - Rapid Res. Let. **4**, 200 (2010).
[18]H. Y. Niu, P. Y. Wei, Y. Sun, X.-Q. Chen, C. Franchini., D. Z. Li, and Y. Y. Li, Appl. Phys. Lett. **99**, 031901 (2011).
[19]Q. Zhu, A. R. Oganov, M. A. Salvadó, P. Pertierra, and A. O. Lyakhov, Phys. Rev. B **83**, 193410 (2011).
[20]J. B. Levine, S. H. Tolbert, and R. B. Kaner, Adv. Funct. Mater **19**, 3519 (2009).
[21]P. F. Mcmillan, Nat. Mat. **1**, 19 (2002).
[22]J. B. Levine, J. B. Betts, J. D. Garrett, S. Q. Guo, J. T. Eng, A. Migliori, and R. B. Kaner, Acta Mater. **58**, 1530 (2010).
[23]H.-Y. Chung, M. B. Weinberger, J. B. Levine, A. Kavner, J.-M. Yang, and S. H. Tolbert, Science **316**, 436 (2007).
[24]J. B. Levine, S. L. Nguyen, H. I. Rasool, J. A. Wright, S. E. Brown, and R. B. Kaner, J. Am. Chem. Soc. **130**, 16953 (2008).
[25]A. N. Kolmogorov, S. Shah, E. R. Margine, A. F. Bialon, T. Hammerschmidt, and R. Drautz, Phys. Rev. Lett. **105**, 217003 (2010).
[26]A. F. Bialon, T. Hammerschmidt, R. Drautz, S. Shah, E. R. Margine, and A. N. Kolmogorov, Appl. Phys. Lett. **98**, 081901 (2011).
[27]J. P. Perdew, K. Burke, and M. Ernzerhof, Phys. Rev. Lett. **77**, 3865 (1996).
[28]P. E. Blöchl, Phys. Rev. B **50**, 17953 (1994).
[29]G. Kresse and J. Hafner, Phys. Rev. B **47**, 558 (1993).
[30]G. Kresse and J. Furthmüller, Phys. Rev. B **54**, 11169 (1996).
[31]X.-Q. Chen, H. Y. Niu, D. Z. Li, and Y. Y. Li, Intermetallics **19**, 1275 (2011).
[32]X.-Q. Chen, H. Y. Niu, C. Franchini, D. Z. Li, and Y. Y. Li, Phys. Rev. B **84**, 121405(R) (2011).
[33]S. Andersson, and T. Lundström, Acta Chem. Scand. **22**, 3103 (1968).
[34]H. B. Xu, Y. X. Wang, and V. C. Lo, Phys. Stat. Sol. (RRL) - Rapid Res. Let. **5**, 13 (2011).
[35]B. Silvi and A. Savin, Nature (London) **371**, 683 (1994).
[36]J. Rodrüez-Carvajal, Physica B **192**, 55 (1993).
[37]O. Beckstein, J. E. Klepeis, G. L. W. Hart, and O. Pankratov, Phys. Rev. B **63**, 134112 (2001).
[38]D. Roundy, C. R. Krenn, M. L. Cohen, and J. W. Jr. Morris, Philos. Mag. A **81**, 1725 (2001).
[39]D. Roundy, C. R. Krenn, M. L. Cohen, and J. W. Morris Jr., Phys. Rev. Lett. **82**, 2713 (1999).
[40]S.-H. Jhi, S. G. Louie, M. L. Cohen, and J. W. Morris Jr., Phys. Rev. Lett. **87**, 075503 (2001).
[41]D. G. Pettifor, *Bonding and Structure of Molecules and Solids* (Oxford University Press, Oxford, 1995).
[42]J. K. Burdett and S. Lee, J. Am. Chem. Soc. **107**, 3063 (1985).
[43]W. Tang, E. Sanville, and G. Henkelman, J. Phys.: Condens. Matter **21**, 084204 (2009).
[44]S. F. Pugh, Philos. Mag. Ser. **45**, 823 (1954).
[45]R. F. Zhang, S. Veprek, and A. S. Argon, Appl. Phys. Lett. **91**, 201914 (2007).
[46]X.-Q. Chen, C. L. Fu, M. Krčmar, and G. S. Painter, Phys. Rev. Lett. **100**, 196403 (2008).
[47]P. Lazar and R. Podloucky, Phys. Rev. B **78**, 104114 (2008).
[48]S. Grasso, C. Hu, O. Vasylkiv, T. S. Suzuki, S. Guo, T. Nishimura, and Y. Sakka, Scr. Mater. **64**, 256 (2011).
[49]T. B. Massalski and H. Okamoto, *Binary Alloy Phase Diagrams*, 2nd ed. (ASM International, Material Park, Ohio, 1990).
[50]P. S. Kislyi, *Superhard and Refractory Materials* (Institute of Superhard Materials, Kiev, 1985), p. 86.
[51]H. Y. Gou, Z. P. Li, F. M. Gao, J. W. Zhang, R. C. Ewing, and J. Lian, Appl. Phys. Lett. **100**, 111907 (2012).
[52]A. Knappschneider, C. Litterscheid, J. Kurzman, R. Seshadri, and B. Albert, Inorg. Chem. **50**, 10540 (2011).